

Superstretchable Elastomer from Cross-linked Ring Polymers

Jiuling Wang¹, Thomas C. O'Connor², Gary S. Grest³, and Ting Ge^{1,*}

¹*Department of Chemistry and Biochemistry, University of South Carolina, Columbia, South Carolina 29208, USA*

²*Department of Materials Science and Engineering, Carnegie Mellon University, Pittsburgh, Pennsylvania 15213, USA*

³*Sandia National Laboratories, Albuquerque, New Mexico 87185, USA*

 (Received 21 January 2022; accepted 20 May 2022; published 9 June 2022)

The stretchability of polymeric materials is critical to many applications such as flexible electronics and soft robotics, yet the stretchability of conventional cross-linked linear polymers is limited by the entanglements between polymer chains. We show using molecular dynamics simulations that cross-linked ring polymers are significantly more stretchable than cross-linked linear polymers. Compared to linear polymers, the entanglements between ring polymers do not act as effective cross-links. As a result, the stretchability of cross-linked ring polymers is determined by the maximum extension of polymer strands between cross-links, rather than between trapped entanglements as in cross-linked linear polymers. The more compact conformation of ring polymers before deformation also contributes to the increase in stretchability.

DOI: [10.1103/PhysRevLett.128.237801](https://doi.org/10.1103/PhysRevLett.128.237801)

Cross-linked elastomers are widely used as both flexible soft materials and highly deformable matrices for polymer composites. Elastomers are distinguished from metallic, ceramic, and other amorphous materials by their ability to reversibly accommodate large stretches ($\sim 100\%$ – 500%). This makes them ideal for applications in soft robotics [1], wearable electronics [2,3], and biomedical devices [4]. However, elastomer softness and stretchability are limited by the tendency of polymer chains to form entanglements that topologically hinder the motion of network strands. Most polymers naturally form a dense network of entanglements at equilibrium, which dominate both the stiffness and stretchability of an elastomer if the entanglement density is higher than the cross-link density [5]. Achieving ultrasoft and stretchable elastomers requires overcoming the barrier produced by polymer entanglements.

One promising route toward reducing the entanglement density and enhancing the stretchability of elastomers is by controlling polymer chain topology through advances in chemical synthesis [6]. This is exemplified by the supersoft elastomers recently made from cross-linked bottle-brush polymers [7–10], in which the side chains expand the effective diameter of the network strands and reduce the number of trapped entanglements. In this Letter, we investigate an alternative scheme based on the unique properties of nonconcatenated ring polymers. The topological constraints of nonconcatenation force the ring polymers to have loopy and globular conformations [11–15]. However, these topological constraints evolve with time in a self-similar manner [14,16] such that there is no apparent entanglement network that strongly confines the dynamics of chains at any specific scale. As a result,

nonconcatenated ring polymers possess distinctive linear [17,18] and nonlinear [19–21] rheology. As we will show, the absence of an entanglement network in ring polymer melts offers a novel pathway to create ultrasoft and stretchable elastomers.

We use molecular dynamics simulations to generate and study the mechanics of ring polymer elastomers with precisely controlled topology. We show that nonconcatenated ring elastomers exhibit dramatically higher stretchability than conventional cross-linked linear polymers with the same degree of polymerization. The superior stretchability is related to both the absence of an entanglement network in ring polymers and the more compact conformations of ring polymers in the undeformed state.

Polymers are modeled with the common bead-spring model [22], which has been used previously to simulate the static and dynamic properties of nonconcatenated ring polymer melts [23,24]. All monomers interact via the truncated and shifted Lennard-Jones potential with cutoff $r_c = 2.5 \sigma$, while chains of N monomers each are connected by the finite extensible nonlinear elastic (FENE) bonding potential. A bond bending potential with a stiffness 1.5ϵ is used to adjust the entanglement length of linear chains to $N_e = 28$ beads [25,26]. The entanglement time $\tau_e \approx 4 \times 10^3 \tau$ [27], which is the relaxation time of an entanglement strand of linear chains.

Ring polymer melts of length $N = 400, 800,$ and $1600,$ and linear polymer melts of $N = 800$ were well equilibrated at temperature $T = 1.0 \epsilon/k_B$ and monomer number density $\rho = 0.89 \sigma^{-3}$. The number of ring polymers is $M = 1600, 1200,$ and 600 for $N = 400, 800,$ and $1600,$ respectively. There are $M = 1600$ chains in the linear polymer melt with $N = 800$. The melt temperature is

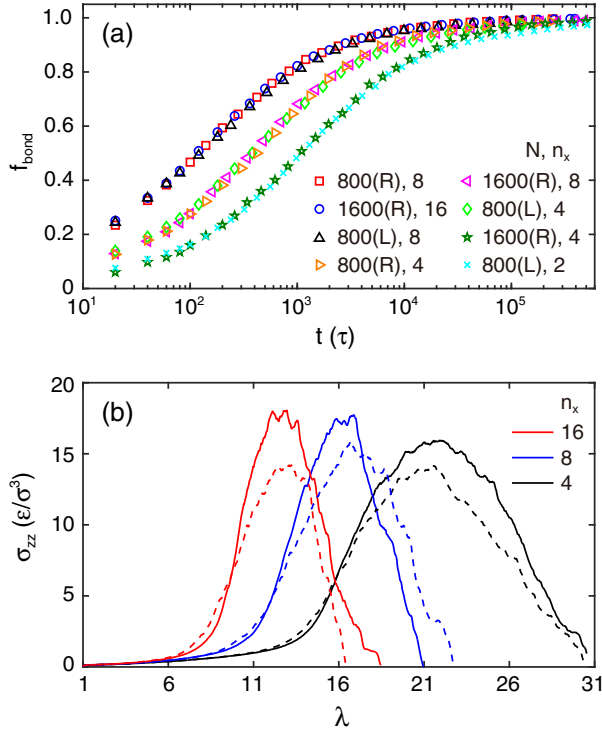


FIG. 1. (a) f_{bond} as a function of time t for the ring (R) and linear (L) polymers of length N and number of cross-links per chain n_x listed in inset. (b) Tensile stress σ_{zz} as a function of stretch ratio λ for randomly cross-linked rings (dashed lines) and kinetically cross-linked rings with regularly spaced cross-linkable monomers (solid lines) for $N = 1600$ and indicated n_x .

maintained by a Nosé-Hoover thermostat with a characteristic damping time of 1τ .

To demonstrate the robustness of ring elastomer properties, we use two methods to cross-link the ring polymer melts. In one method, we randomly pick two monomers that are separated by less than 1.1σ and link them by a FENE bond. We make sure that any two cross-links are separated by no fewer than 10 bonds along the contour of the same ring. In the other method, we preselect monomers that are regularly distributed along the contour of a ring polymer and allow FENE bonds to kinetically form between two such monomers over time. Each of these cross-linkable monomers can form at most one new bond with another cross-linkable monomer, when the distance between two cross-linkable monomers is smaller than 1.3σ . We track f_{bond} , the ratio of the number of newly created bonds to the maximum number of bonds that may be created. f_{bond} increases with time as shown in Fig. 1(a). The time dependence of f_{bond} does not depend on the length N of ring polymers. Instead, it depends only on the number of cross-links per chain n_x . Notably, the time dependence is almost identical for the ring and linear polymers with the same n_x . The reason is that the average spacing between the cross-linkable monomers, which is 3.8σ , 4.8σ , and 6.1σ for $n_x = 16$, 8, and 4, respectively,

is smaller or at most comparable to the average spacing 5σ between entanglements, and thus the kinetics of two cross-linkable monomers finding each other is controlled by the same unentangled dynamics of local chain segments. In both methods, we do not control inter vs intrachain cross-links, as in typical experiments that only control the density of cross-links. The fraction of interchain cross-links is shown in the Supplemental Material [28].

We characterize the mechanics of the cross-linked elastomers by deforming them in uniaxial elongation. To enable the mechanical failure of backbone bonds at large strain, we replace the unbreakable FENE bonds with breakable quartic bonds [29–33]. The equilibrium bond length of quartic bonds is the same as that of FENE bonds. As for the FENE bonds, the quartic bonds prevent the polymers from crossing and preserve the topological constraints, but quartic bonds break at a tension $240\epsilon/\sigma$, or ~ 100 larger than the van der Waals forces.

The uniaxial elongation is performed at a constant strain rate in the z direction, while the stress components σ_{xx} and σ_{yy} in the x and y directions are kept zero using a Nosé-Hoover barostat with a characteristic time 10τ . During the deformation, the temperature is maintained at $T = 1.0\epsilon/k_B$ using a Nosé-Hoover thermostat with a characteristic time 1τ . More details of the simulation protocols are provided in the Supplemental Material [28]. All the simulations were performed by using the LAMMPS package [34,35].

The tensile stress σ_{zz} as a function of the stretch ratio λ , which is the box size L_z along the z direction divided by the value L_z^0 before the deformation, is plotted in Fig. 1(b) for different systems. Each stress-strain curve consists of an initial linear elastic regime, a regime of nonlinear stress increase, and a decrease of the stress after reaching the ultimate strength. For the same n_x , the stress-strain curves of the randomly and kinetically cross-linked systems are similar. In the rest of this Letter, we present the results only for the randomly cross-linked systems.

To reveal the effects of polymer topology on the stretchability of cross-linked polymers, we randomly cross-linked entangled linear polymer melts, and compared the behaviors of cross-linked linear and ring polymers. The number of monomers S between two cross-links in the ring and linear polymers with $N = 800$ and $n_x = 8$ are compared in Fig. S1 in the Supplemental Material [28]. For the ring polymers, the average spacing between cross-links $\bar{S} = 100$ is equal to N/n_x . For the linear polymers, $\bar{S} = 89$ due to the presence of dangling chain ends. The absence of dangling ends is one advantage of cross-linked ring polymers compared with the cross-linked linear polymers in conventional elastomers.

Figure 2 compares the stress-strain curves of the cross-linked ring and linear polymers with $N = 800$ at strain rate $10^{-4}\tau^{-1}$. The points where bonds start to break are indicated by the cross symbols. The subsequent increase

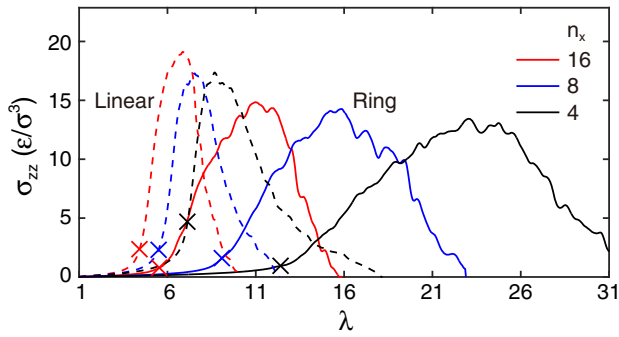


FIG. 2. Tensile stress σ_{zz} as a function of stretch ratio λ for randomly cross-linked ring (solid lines) and linear polymer melts (dashed lines) with $N = 800$. The red, blue, and black lines are for $n_x = 16, 8,$ and 4 , respectively. The cross symbols indicate λ at which the bonds begin to break. Deformation rate is $10^{-4} \tau^{-1}$.

in the fraction of broken bonds out of all bonds f_{broken} is shown in Fig. S2 in the Supplemental Material [28]. For the same n_x , the ring polymers are significantly more stretchable than the linear polymers, as reflected in the larger values of λ for the end of the initial elastic regime, the emergence of broken bonds, and the stress peak for the ultimate strength. Figure S3 in the Supplemental Material [28] shows the intrachain cross-links have negligible effects on the stretchability of elastomers. Figure S4 in the Supplemental Material [28] shows the stretchability of cross-linked ring polymers slightly changes as the deformation rate varies by 2 orders of magnitude. The highest rate $10^{-3} \tau^{-1}$ is 4 times τ_e^{-1} , while the slower rates $10^{-4} \tau^{-1}$ and $10^{-5} \tau^{-1}$ are both smaller than τ_e^{-1} , allowing the adjustment of entanglements.

Gels of cross-linked cyclic polymers have been synthesized in experiments and compared with the gels of cross-linked linear polymers in terms of both swelling behavior and mechanical properties [36,37]. The higher swelling ratio and the higher strain at the breaking point are consistent with the observation of the higher stretchability of cross-linked ring polymers in our simulations.

As the cross-linking density decreases from $n_x = 16$ to $n_x = 4$, the increase of the stretchability is more prominent in the ring polymers compared to that in the linear polymers. This suggests that the stretchability of cross-linked linear polymers is controlled by the trapped entanglements [5,38] and thus not strongly affected by the reduction in n_x . By contrast, the stretchability of cross-linked ring polymers is controlled by the strands between cross-links and only depends on n_x .

According to the elasticity theory of cross-linked linear polymers [39], the network shear modulus G is proportional to the sum of the number densities of cross-links and entanglements, which act as effective cross-links, i.e., $G \sim (1/\bar{S} + 1/N_e)$. For the cross-linked linear polymers of $N = 800$, following the standard protocol established for the entropic elasticity of Gaussian linear chains [39], we

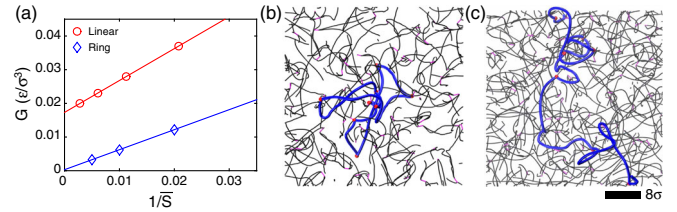


FIG. 3. (a) Shear modulus G as a function of $1/\bar{S}$ for randomly cross-linked linear and ring polymers of length $N = 800$. Snapshots of randomly cross-linked (b) ring and (c) linear polymers of $N = 800$ with monomer positions averaged over a period of $4 \times 10^5 \tau$ for a region of size $40 \sigma \times 40 \sigma \times 10 \sigma$. The cross-links with $n_x = 8$ are fixed during the simulations to obtain the averaged monomer positions. One polymer (blue) and the associated cross-links (red spheres) are highlighted, while other polymers (gray) and the associated cross-links (magenta) are shown as a dimmed background.

extract G from the linear regime of the stress-strain curve as $G = \sigma_{zz}/(\lambda^2 - 1/\lambda)$. Figure 3(a) shows G as a function of $1/\bar{S}$. As expected, G scales linearly with $1/\bar{S}$. The value $G_e = 0.017 \epsilon/\sigma^3$ at vanishing $1/\bar{S}$ corresponds to the contribution from the entanglement network. At the highest cross-linking density of $n_x = 16$ with $1/\bar{S} \approx 0.02$, G_e is about 1/2 of G . At lower cross-linking densities, G_e is more than 1/2 of G and dominates over the contribution from the cross-links. A similar linear dependence of G on the inverse of network strand length was observed in the simulations of end-linked polymer networks by Duering *et al.* [38].

Despite of the loopy globular conformation, the end-to-end vector of a section in a ring polymer also follows the Gaussian distribution, as shown in Fig. S5 in the Supplemental Material [28]. Therefore, the shear modulus G may be extracted using the same protocol for linear chains. As shown in Fig. 3(a), G for cross-linked rings also scales linearly with $1/\bar{S}$, but approaches 0 at vanishing $1/\bar{S}$ due to the absence of an entanglement network. At all cross-linking densities, G is solely determined by the cross-links with no entanglements acting as effective cross-links. This result is consistent with the absence of a rubbery plateau in the stress relaxation function for the nonconcatenated ring polymer melts studied here [24]. It also demonstrates that the strain rate in the simulations is sufficiently slow for a response near the thermal equilibrium. Figure S6 in the Supplemental Material [28] shows that there is a finite modulus at vanishing $1/\bar{S}$ for a higher strain rate $10^{-3} \tau^{-1}$, at which some entanglements contribute to G as a response out of equilibrium [40]. Examination of the unreleased topological constraints at high strain rates and their relations to the slow dynamics in the undeformed state [41–43] is an intriguing topic for future research.

Generally, the shear modulus and the stretchability are inversely correlated for cross-linked linear polymers [10].

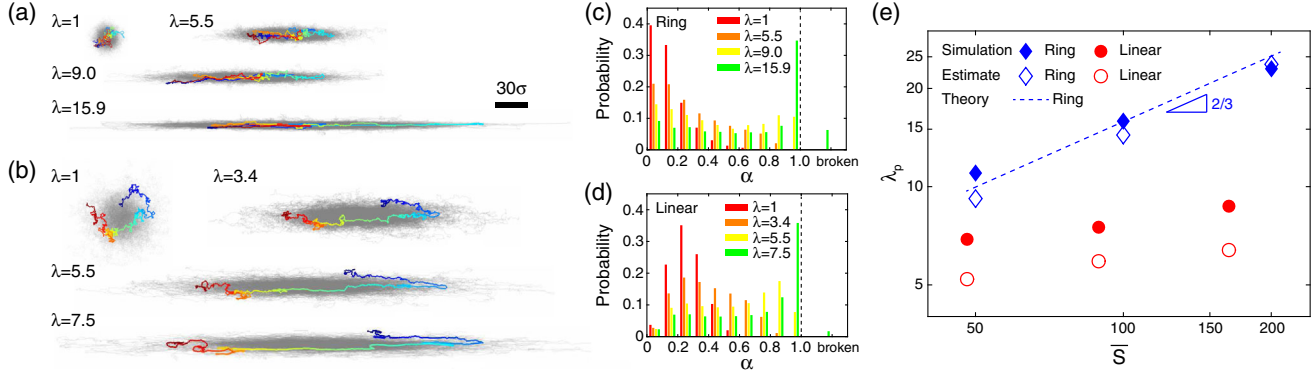


FIG. 4. Snapshots of randomly cross-linked (a) ring and (b) linear polymer melts of $N = 800$ and $n_x = 8$ at indicated λ . The centers of mass of the polymers are shifted to overlap. One polymer is highlighted with the monomers colored based on their positions along the polymer contour. The radius of gyration of the highlighted polymer is closest to the mean value for all the polymers at $\lambda = 1$. Probability distributions of the degree of tautness α for (c) the strands between cross-links in the ring polymers and (d) the strands with $S^* = 32$ monomers per strand in the linear polymers. (e) Stretch ratio at the stress peak λ_p as a function of \bar{S} . Filled symbols are from the stress-strain curves in Fig. 2. Open symbols are estimates using $\sqrt{3}\lambda_{\max}$, where λ_{\max} is the maximum extension of network strands. Dashed line is the best fit to the scaling relation in Eq. (1).

This inverse correlation is also observed for the cross-linked ring polymers. Along with the superstretchability, the cross-linked ring polymers exhibit supersoftness. As shown in Fig. 3(a), G of cross-linked ring polymers, which is controlled by the cross-linking density, is significantly lower than that of cross-linked linear polymers. In experiments, this reduction would bring G from the typical range 0.1–1 MPa down to 1–100 kPa [7,9], which is desirable for biocompatibility with natural tissues and organs.

The contrasting effects of entanglements on the cross-linked ring and linear polymers are visualized in Figs. 3(b),(c). The entanglements between cross-linked polymers are inherited from those in the polymer melt. Time averaging the positions of monomers with the cross-links fixed in space reveals the underlying entanglements. The time averaging over a period of $4 \times 10^5 \tau \approx 100 \tau_e$ leads to a dense entanglement network in the linear polymers, as the dynamics of entangled linear polymers are confined in tubelike regions [39]. By contrast, after the same period of time averaging, there is a sparser network in the ring polymers, as the self-similar dynamics of entangled ring polymers progressively reduces the number of entanglements [14,44]. Primitive path analysis [25] yields similar results for the ring and linear polymers, as shown in Fig. S7 in the Supplemental Material [28].

On the molecular level, a polymer chain becomes taut upon stretching. A visual comparison of the stretching of one chain in the cross-linked ring and linear polymers is shown in Fig. 4 for $N = 800$ and $n_x = 8$. At $\lambda = 1$, the ring polymers are more compact than the linear polymers. The three values of $\lambda > 1$ shown correspond to the end of the linear elastic regime, the emergence of broken bonds, and at the stress peak.

For cross-linked linear polymers, the density of effective cross-links is significantly increased by the

trapped entanglements, and the number of monomers S^* between effective cross-links is much smaller than \bar{S} . The stretchability is determined by the maximum extension of a network strand between effective cross-links $\lambda_{\max}^L = l_s^*/d_s^* = (S^*/C_\infty)^{1/2}$, where $l_s^* = S^*l_0$ and $d_s^* = (C_\infty S^* l_0^2)^{1/2}$ are the contour length and the rms end-to-end distance of a network strand as an ideal random-walk chain with average bond length $l_0 = 0.96 \sigma$ and characteristic ratio $C_\infty = 2.8$ [45]. Using the relation $G = \rho k_B T / S^*$ according to the classical polymer elasticity theory [39], we estimate that $S^* = 25, 32$, and 39 , and thus $\lambda_{\max}^L = 3.0, 3.4$, and 3.7 for $N = 800$ and $n_x = 16, 8$, and 4 , respectively.

In the undeformed state, the end-to-end vectors of network strands are randomly orientated with respect to the stretching direction. As a result, only a small fraction of network strands with their initial orientations close to the stretching direction can reach the maximum extension at $\lambda = \lambda_{\max}^L$. This is demonstrated by the probability distribution of the degree of tautness $\alpha^L = d_s^*/l_s^*$ of the network strands at $\lambda = \lambda_{\max}^L$ in Fig. 4(d). (Details of measuring α are provided in the Supplemental Material [28].) With further stretching, more strands become taut ($\alpha = 1$) and more bonds break, as shown in Fig. 4(d). Since the average projection of initial effective network strands to the stretching direction is $d_s^*/\sqrt{3}$, λ_p^L at the stress peak is estimated as $\sqrt{3}\lambda_{\max}^L = 5.2, 5.9$, and 6.4 , which are good approximations (within 30% deviation) of the simulation results $\lambda_p^L = 6.9, 7.5$, and 8.7 in Fig. 2, as compared in Fig. 4(e).

For cross-linked ring polymers, the stretchability is controlled by the maximum extension of a network strand between cross-links $\lambda_{\max}^R = l_s/d_s$, where $l_s = \bar{S}l_0$ and d_s are the contour length and rms end-to-end distance of a network strand. For $\bar{S} = 50, 100$, and 200 , $d_s = 9.0 \sigma$,

11.5 σ , and 14.0 σ , following the scaling $d_s \sim \bar{S}^{1/3}$ for a loopy globular conformation [14], which gives $\lambda_{\max}^R = 5.3$, 8.3, and 13.7, respectively. Similar to the results for the linear polymers, at $\lambda = \lambda_{\max}^R$, only a small fraction of the network strands are taut [Fig. 4(c)]. The stretch ratio at the stress peak λ_p^R is estimated as $\sqrt{3}\lambda_{\max}^R = 9.2$, 14.4, and 23.7 for the three systems, which deviate from the simulation results $\lambda_p^R = 11.0$, 15.9, and 23.0 in Fig. 2 by less than 20%, as shown in Fig. 4(e).

On the scaling level, $d_s \approx (\bar{S}/N_e)^{1/3}(N_e^{1/2}l_0)$ for the rings in loopy globular conformations [14]. Here, N_e denotes the length scale comparable to the entanglement length in linear polymers, above which $d_s \sim \bar{S}^{1/3}$ due to the topological constraints [13,14,46]. The maximum stretchability of cross-linked rings scales with \bar{S} and N_e as

$$\lambda_{\max}^R \approx \left(\frac{\bar{S}}{N_e}\right)^{2/3} N_e^{1/2}. \quad (1)$$

The scaling relation in Eq. (1) allows us to fit λ_p^R to $c(\bar{S}/N_e)^{2/3}N_e^{1/2}$ with $N_e = 28$. The fitting result is $c = 1.28 \pm 0.07$, and the best fit is shown by the dashed line in Fig. 4(e). In the limit of $\bar{S} \gg N_e$, the effective network strand length of cross-linked linear polymers $S^* \approx N_e$, as the dilute cross-links are negligible compared to the entanglements. Therefore, $\lambda_{\max}^L \approx N_e^{1/2}$, where C_∞ is dropped for scaling analysis. As shown in Fig. 4(e), the simulation data of λ_p^L are not in the \bar{S} -independent asymptotic regime, though the \bar{S} dependence is weak.

The relative increase of the stretchability of cross-linked rings with respect to cross-linked linear chains is $\lambda_{\max}^R/\lambda_{\max}^L \approx (\bar{S}/N_e)^{2/3}$ for $\bar{S} \gg N_e$. If the network strand of cross-linked rings were an ideal random-walk (RW) chain, the maximum extension $\lambda_{\max}^{R,RW} \approx \bar{S}^{1/2}$, which is larger than λ_{\max}^L only by $(\bar{S}/N_e)^{1/2}$. The factor $\lambda_{\max}^R/\lambda_{\max}^{R,RW} \approx (\bar{S}/N_e)^{1/6}$ quantifies the additional contribution from the more compact equilibrium conformations of rings.

We have shown that cross-linked ring polymers are a viable and robust route to generate superstretchable elastomers. Unlike linear chains, nonconcatenated rings do not form a network of trapped entanglements even when N is large, allowing ring elastomers to overcome the entanglement barrier that limits the stretchability of other elastomer architectures. In addition to the superstretchability, the cross-linked ring polymers exhibit superior softness with reduced shear modulus. These superior properties are rooted in the loopy globular conformations and self-similar dynamics of the nonconcatenated rings. Given recent advances in reversible polymerization of nonconcatenated ring polymers [47–49], our results provide a timely and compelling demonstration of how ring polymers could be used to create practical and sustainable materials [50]. We suspect these materials could be made even more

stretchable by incorporating reversible and exchangeable cross-links within the network [51–53].

T. G. acknowledges start-up funds from the University of South Carolina. T. O. acknowledges start-up funds from Carnegie Mellon University. This work was supported in part by the National Science Foundation EPSCoR Program under NSF Grant No. OIA-1655740. Any opinions, findings and conclusions, or recommendations expressed in this material are those of the authors and do not necessarily reflect those of the National Science Foundation. Computational resources were provided by University of South Carolina flagship computing cluster Hyperion. This research used resources at the National Energy Research Scientific Computing Center (NERSC), a U.S. Department of Energy Office of Science User Facility operated under Contract No. DE-AC02-05CH11231. These resources were obtained through the Advanced Scientific Computing Research (ASCR) Leadership Computing Challenge (ALCC). This work was performed, in part, at the Center for Integrated Nanotechnologies, an Office of Science User Facility operated for the U.S. Department of Energy (DOE) Office of Science. Sandia National Laboratories is a multi-mission laboratory managed and operated by National Technology & Engineering Solutions of Sandia, LLC, a wholly owned subsidiary of Honeywell International, Inc., for the U.S. DOE's National Nuclear Security Administration under Contract No. DE-NA-0003525. The views expressed in the Letter do not necessarily represent the views of the U.S. DOE or the U.S. Government.

*Corresponding author.

tingg@mailbox.sc.edu

- [1] J. Z. Gul, M. Sajid, M. M. Rehman, G. U. Siddiqui, I. Shah, K.-H. Kim, J.-W. Lee, and K. H. Choi, *Sci. Technol. Adv. Mater.* **19**, 243 (2018).
- [2] M. Amjadi, K. Kyung, I. Park, and M. Sitti, *Adv. Funct. Mater.* **26**, 1678 (2016).
- [3] W. Wu, *Sci. Technol. Adv. Mater.* **20**, 187 (2019).
- [4] J. C. Yeo and C. T. Lim, *Microsyst. Nanoeng.* **2**, 16043 (2016).
- [5] D. S. Pearson and W. W. Graessley, *Macromolecules* **13**, 1001 (1980).
- [6] Y. Gu, J. Zhao, and J. A. Johnson, *Angew. Chem. Int. Ed.* **59**, 5022 (2020).
- [7] L. Cai, T. E. Kodger, R. E. Guerra, A. F. Pegoraro, M. Rubinstein, and D. A. Weitz, *Adv. Mater.* **27**, 5132 (2015).
- [8] Z. Cao, J.-M. Y. Carrillo, S. S. Sheiko, and A. V. Dobrynin, *Macromolecules* **48**, 5006 (2015).
- [9] W. F. M. Daniel, J. Burdyńska, M. Vatankhah-varmoosfaderani, K. Matyjaszewski, J. Paturej, M. Rubinstein, A. V. Dobrynin, and S. S. Sheiko, *Nat. Mater.* **15**, 183 (2016).
- [10] S. S. Sheiko and A. V. Dobrynin, *Macromolecules* **52**, 7531 (2019).
- [11] S. Obukhov, A. Johner, J. Baschnagel, H. Meyer, and J. Wittmer, *Europhys. Lett.* **105**, 48005 (2014).

- [12] S. Gooßen, A. R. Brás, M. Krutyeva, M. Sharp, P. Falus, A. Feoktystov, U. Gasser, W. Pyckhout-Hintzen, A. Wischnewski, and D. Richter, *Phys. Rev. Lett.* **113**, 168302 (2014).
- [13] A. Rosa and R. Everaers, *Phys. Rev. Lett.* **112**, 118302 (2014).
- [14] T. Ge, S. Panyukov, and M. Rubinstein, *Macromolecules* **49**, 708 (2016).
- [15] M. Kruteva, J. Allgaier, M. Monkenbusch, L. Porcar, and D. Richter, *ACS Macro Lett.* **9**, 507 (2020).
- [16] M. Kruteva, M. Monkenbusch, J. Allgaier, O. Holderer, S. Pasini, I. Hoffmann, and D. Richter, *Phys. Rev. Lett.* **125**, 238004 (2020).
- [17] M. Kapnistos, M. Lang, D. Vlassopoulos, W. Pyckhout-Hintzen, D. Richter, D. Cho, T. Chang, and M. Rubinstein, *Nat. Mater.* **7**, 997 (2008).
- [18] R. Pasquino, T. C. Vasilakopoulos, Y. C. Jeong, H. Lee, S. Rogers, G. Sakellariou, J. Allgaier, A. Takano, A. R. Brás, T. Chang, S. Gooßen, W. Pyckhout-Hintzen, A. Wischnewski, N. Hadjichristidis, D. Richter, M. Rubinstein, and D. Vlassopoulos, *ACS Macro Lett.* **2**, 874 (2013).
- [19] Q. Huang, J. Ahn, D. Parisi, T. Chang, O. Hassager, S. Panyukov, M. Rubinstein, and D. Vlassopoulos, *Phys. Rev. Lett.* **122**, 208001 (2019).
- [20] T. C. O'Connor, T. Ge, M. Rubinstein, and G. S. Grest, *Phys. Rev. Lett.* **124**, 027801 (2020).
- [21] D. Parisi, S. Costanzo, Y. Jeong, J. Ahn, T. Chang, D. Vlassopoulos, J. D. Halverson, K. Kremer, T. Ge, and M. Rubinstein, *Macromolecules* **54**, 2811 (2021).
- [22] K. Kremer and G. S. Grest, *J. Chem. Phys.* **92**, 5057 (1990).
- [23] J. D. Halverson, W. B. Lee, G. S. Grest, A. Y. Grosberg, and K. Kremer, *J. Chem. Phys.* **134**, 204904 (2011).
- [24] J. D. Halverson, W. B. Lee, G. S. Grest, A. Y. Grosberg, and K. Kremer, *J. Chem. Phys.* **134**, 204905 (2011).
- [25] R. Everaers, S. K. Sukumaran, G. S. Grest, C. Svaneborg, A. Sivasubramanian, and K. Kremer, *Science* **303**, 823 (2004).
- [26] G. S. Grest, *J. Chem. Phys.* **145**, 141101 (2016).
- [27] T. Ge, M. O. Robbins, D. Perahia, and G. S. Grest, *Phys. Rev. E* **90**, 012602 (2014).
- [28] See Supplemental Material at <http://link.aps.org/supplemental/10.1103/PhysRevLett.128.237801> for characterization of the simulation samples, protocols of the deformation, and analysis of the simulation results.
- [29] M. J. Stevens, *Macromolecules* **34**, 2710 (2001).
- [30] J. Rottler, S. Barsky, and M. O. Robbins, *Phys. Rev. Lett.* **89**, 148304 (2002).
- [31] T. Ge, F. Pierce, D. Perahia, G. S. Grest, and M. O. Robbins, *Phys. Rev. Lett.* **110**, 098301 (2013).
- [32] J. Wang and T. Ge, *Macromolecules* **54**, 7500 (2021).
- [33] C. W. Barney, Z. Ye, I. Sacligil, K. R. McLeod, H. Zhang, G. N. Tew, R. A. Riggleman, and A. J. Crosby, *Proc. Natl. Acad. Sci. U.S.A.* **119**, e2112389119 (2022).
- [34] A. P. Thompson, H. M. Aktulga, R. Berger, D. S. Bolintineanu, W. M. Brown, P. S. Crozier, P. J. in 't Veld, A. Kohlmeyer, S. G. Moore, T. D. Nguyen, R. Shan, M. J. Stevens, J. Tranchida, C. Trott, and S. J. Plimpton, *Comput. Phys. Commun.* **271**, 108171 (2022).
- [35] A. P. Thompson, S. J. Plimpton, and W. Mattson, *J. Chem. Phys.* **131**, 154107 (2009).
- [36] K. Zhang, M. A. Lackey, J. Cui, and G. N. Tew, *J. Am. Chem. Soc.* **133**, 4140 (2011).
- [37] L. Trachsel, M. Romio, M. ZenobiWong, and E. M. Benetti, *Macromol. Rapid Commun.* **42**, 2000658 (2021).
- [38] E. R. Duering, K. Kremer, and G. S. Grest, *J. Chem. Phys.* **101**, 8169 (1994).
- [39] M. Rubinstein and R. H. Colby, *Polymer Physics* (Oxford University Press, New York, 2003).
- [40] A recent simulation [32] has shown that in the glassy state of ring polymers, which is far from equilibrium, a fraction of entanglements forms a network that supports the stable growth of craze fibrils.
- [41] D. G. Tsalikis, V. G. Mavrantzas, and D. Vlassopoulos, *ACS Macro Lett.* **5**, 755 (2016).
- [42] D. Michieletto, N. Nahali, and A. Rosa, *Phys. Rev. Lett.* **119**, 197801 (2017).
- [43] J. Smrek, K. Kremer, and A. Rosa, *ACS Macro Lett.* **8**, 155 (2019).
- [44] D. Michieletto and T. Sakaue, *ACS Macro Lett.* **10**, 129 (2021).
- [45] H.-P. Hsu and K. Kremer, *J. Chem. Phys.* **144**, 154907 (2016).
- [46] M. Lang, *Macromolecules* **46**, 1158 (2013).
- [47] E. C. Feinberg, H. L. Hernandez, C. L. Plantz, E. B. Mejia, N. R. Sottos, S. R. White, and J. S. Moore, *ACS Macro Lett.* **7**, 47 (2018).
- [48] E. M. Lloyd, H. Lopez Hernandez, E. C. Feinberg, M. Yourdkhani, E. K. Zen, E. B. Mejia, N. R. Sottos, J. S. Moore, and S. R. White, *Chem. Mater.* **31**, 398 (2019).
- [49] K. Molnar, H. Kim, D. Chen, C. A. Helfer, G. Kaszas, G. B. McKenna, J. A. Kornfield, C. Yuan, and J. E. Puskas, *Polym. Chem.* **13**, 668 (2022).
- [50] M. Romio, L. Trachsel, G. Morgese, S. N. Ramakrishna, N. D. Spencer, and E. M. Benetti, *ACS Macro Lett.* **9**, 1024 (2020).
- [51] J. Xu, W. Chen, C. Wang, M. Zheng, C. Ding, W. Jiang, L. Tan, and J. Fu, *Chem. Mater.* **30**, 6026 (2018).
- [52] H. Guo, Y. Han, W. Zhao, J. Yang, and L. Zhang, *Nat. Commun.* **11**, 2037 (2020).
- [53] J.-Y. Sun, X. Zhao, W. R. Illeperuma, O. Chaudhuri, K. H. Oh, D. J. Mooney, J. J. Vlassak, and Z. Suo, *Nature (London)* **489**, 133 (2012).